

# Scale-dependent alignment in compressible magnetohydrodynamic turbulence

James R. Beattie\*

*Department of Astrophysical Sciences, Princeton University, Princeton, 08540, NJ, USA*  
*Canadian Institute for Theoretical Astrophysics, University of Toronto, Toronto, M5S3H8, ON, Canada*

Amitava Bhattacharjee

*Department of Astrophysical Sciences, Princeton University, Princeton, 08540, NJ, USA*

(Dated: April 23, 2025)

Using 10,080<sup>3</sup> grid simulations, we analyze scale-dependent alignment in driven, compressible, no net-flux magnetohydrodynamic turbulence. The plasma self-organizes into localized, strongly aligned regions. Alignment spans all primitive variables and their curls. Contrary to incompressible theory, velocity-magnetic alignment scales as  $\theta(\lambda) \sim \lambda^{1/8}$ , where  $\lambda$  is the scale, suggesting a distinct three-dimensional eddy anisotropy and a much higher critical transition scale toward a reconnection-mediated cascade.

## I. INTRODUCTION

Magnetohydrodynamic (MHD) turbulence is ubiquitous in our Universe, whether it be in the solar wind and planetary magnetospheres, or the plasma between galaxy clusters in the intracluster medium. Pertinent to the study of MHD turbulence is the concept of alignment. In strong Alfvénic turbulence, the nonlinear timescale  $t_{nl}$  associated with the MHD cascade rate is set by interactions between counter-propagating shear Alfvén wavepackets  $\mathbf{z}^\mp = \mathbf{u} \mp \mathbf{b}$  that dominantly cascade perpendicular to the magnetic field, where  $\mathbf{b}$  is in velocity units and the symbols have their usual notations. The nonlinear time scale can be estimated as  $t_{nl} \sim 1/(k_\perp z_\perp^\mp \sin \theta)$ , where  $\theta$  is the angle between  $\mathbf{u}$  and  $\mathbf{b}$  [1–7], and in the most extreme case where  $\mathbf{u} = \pm \mathbf{b}$  the Alfvénic cascade can be halted [8].

The  $\mathbf{u}$  and  $\mathbf{b}$  alignment is further a statement about the basic building block of the turbulence – the eddy – which in turbulence models with any alignment are anisotropic in all three dimensions [9], with the relationship between the perpendicular length scales  $(\lambda, \xi)$  set by the alignment angle  $\theta \sim \lambda/\xi$ . With  $t_{nl}$  varying as above, keeping the energy flux  $\epsilon \sim \delta u^2/t_{nl} = \text{const.}$  between the eddies undergoing with  $\delta u \sim \lambda^{1/4} \iff \delta u^2(k_\perp) \sim k_\perp^{-3/2}$  spectrum, means that  $\theta$  has to vary with scale,  $\epsilon \sim \delta u^3 \theta / \lambda = \text{const.} \iff \theta \sim \lambda^{1/4}$  [1, 2, 5]. This means eddies become increasingly sheet-like at small  $\lambda$  (i.e., the turbulent eddy is not rotationally symmetric about the magnetic field). Due to the sheet-like geometry, at a critical  $\lambda_*$  eddies may become tearing-unstable and undergoing a fast, tearing-mediated cascade [10–12]. Hence, the nature of the scale-dependent alignment is critical for connecting MHD turbulence to reconnection and tearing instabilities.

One can attain a highly-aligned  $\mathbf{u}$  and  $\mathbf{b}$  configuration by realizing a minimum energy state [2, 13, 14], or a maximum entropy state [15], through the process of plasma

relaxation due to selective decay. For a relaxation process that preserves the rugged, inviscid, MHD invariants, magnetic helicity,  $H_m = \langle \mathbf{a} \cdot \mathbf{b} \rangle_{\mathcal{V}}$ , where  $\mathbf{b} = \nabla \times \mathbf{a}$  is the vector potential and  $\mathcal{V}$  is a volume containing the turbulent integral scale, and cross helicity,  $H_c = \langle \mathbf{u} \cdot \mathbf{b} \rangle_{\mathcal{V}}$ , this gives  $\mathbf{u} \propto \pm \mathbf{b} \propto \pm \mathbf{j} \propto \pm \boldsymbol{\omega}$ , where  $\mathbf{j} = (1/\mu_0) \nabla \times \mathbf{b}$  is the current density,  $\mu_0$  is the magnetic permittivity and  $\boldsymbol{\omega} = \nabla \times \mathbf{u}$  is the fluid vorticity. Hence, such a process does not only tend to align  $\mathbf{u}$  and  $\mathbf{b}$ , as in dynamical alignment [1, 3], but requires alignment to be spread also across primitive fluid variables  $\mathbf{u}$  and  $\mathbf{b}$  and the respective curls. This is an extended version of Taylor’s global relaxation hypothesis [16], during which the denumerable infinite number of constraints of ideal MHD are replaced by a small number of approximate global invariants, mediated by magnetic reconnection and turbulence. However, most systems do not attain globally relaxed Taylor or Beltrami states, and the question is what a self-organized, partially relaxed state looks like. Since turbulent systems generically exhibit scale-dependence, a first step is to understand the scale-dependent alignment properties of not only  $\mathbf{u}$  and  $\mathbf{b}$  but also  $\mathbf{j}$  and  $\boldsymbol{\omega}$ , which we do for the first time in this study.

In the most extreme case, where the primitive variables and curls are completely aligned, the nonlinear terms in the MHD equations are suppressed and the momentum and magnetic fields completely decouple, i.e., the turbulent nonlinearities  $\mathbf{u} \cdot \nabla \otimes \mathbf{u} = (1/2) \nabla u^2 - \mathbf{u} \times \boldsymbol{\omega}$  becomes an effective isotropic pressure if  $\mathbf{u} \propto \boldsymbol{\omega}$ , and further the induction  $\nabla \times (\mathbf{u} \times \mathbf{b})$  and Lorentz force  $\mathbf{j} \times \mathbf{b}$  tend to zero for  $\mathbf{u} \propto \pm \mathbf{b}$  and  $\mathbf{b} \propto \pm \mathbf{j}$ , respectively. In the maximum entropy framework, such states are sensitive to the energy flux from the turbulent driving source, and may only be observed if there is significant scale-separation between the turbulent outer scale  $\ell_0$  and scales within the cascade [15]. The separation between the inner and outer scale of the turbulence, where the cascade resides, is determined by the plasma Reynolds number  $\text{Re} = u_0 \lambda_0 / \nu$ , where  $\nu$  is the coefficient of kinematic viscosity. For classical Kolmogorov [17] turbulence,  $\lambda_\nu \sim \text{Re}^{3/4} \lambda_0$ , where  $\lambda_\nu$  is the viscous dissipation scale, where the cascade becomes thermally truncated. Hence, to properly measure the

\* james.beattie@princeton.edu

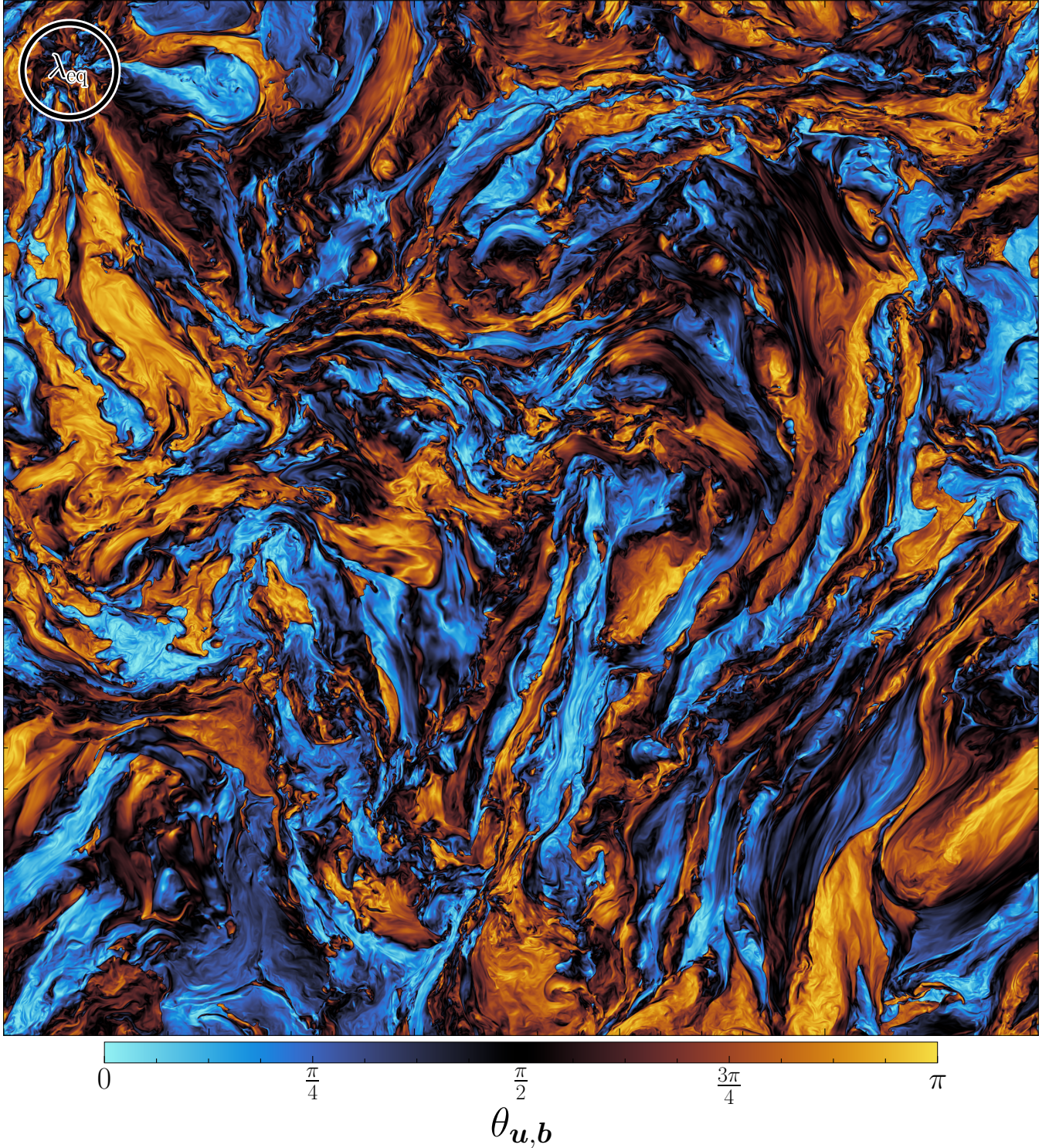


FIG. 1. **The spatial structure of the alignment angle between  $\mathbf{u}$  and  $\mathbf{b}$ .** A two-dimensional slice of the  $\theta_{u,b}$  field, where parallel  $\mathbf{u}$  and  $\mathbf{b}$  are shown in blue  $\theta_{u,b} = 0$ , perpendicular  $\theta_{u,b} = \pi/2$  in black and anti-parallel  $\theta_{u,b} = \pi$  in yellow. The size of the energy equipartition scale,  $\lambda_{\text{eq}}$ , ( $\mathcal{E}_{\text{mag}}(\lambda_{\text{eq}}) = \mathcal{E}_{\text{kin}}(\lambda_{\text{eq}})$ ) is shown in the top left corner. The plasma is self-organized into volume-filling regions of parallel and anti-parallel  $\mathbf{u} \propto \pm \mathbf{b}$  configurations. The perpendicular  $\mathbf{u}$  and  $\mathbf{b}$  configuration, where the Alfvénic nonlinearities in the turbulence are the strongest and hence the cascade is the fastest, are confined to the fractal interfaces between the space-filling parallel and anti-parallel regions.

alignment statistics that are not polluted by driving at  $\ell_0$  or dissipation at  $\ell_\nu$ , we require simulations of  $\text{Re} \gg 1$ .

In this study, we report the volume-integral and scale-dependent alignment statistics from a non-helical, compressible MHD simulation with no net magnetic flux  $\langle \mathbf{b} \rangle_{\mathcal{V}} = \mathbf{0}$ , such that the purely fluctuating magnetic field is maintained by a turbulent dynamo in the saturated state [18–20]. This simulation is novel, in that for the first time for a scale-dependent alignment study, we utilize grid resolutions of  $10,080^3$  (equivalent to  $\text{Rm} \sim \text{Re} \gtrsim 10^6$ ), providing an inertial range in the kinetic energy of roughly three orders of magnitude in length scales (or wavenodes), spanning large-scale supersonic (highly compressible) velocities admitting to  $\mathcal{E}_{\text{kin}}(k) \propto k^{-2}$  and small-scale subsonic (weakly compressible) velocities admitting to  $\mathcal{E}_{\text{kin}}(k) \propto k^{-3/2}$ , where  $\mathcal{E}_{\text{kin}}(k)$  is the kinetic energy power spectrum. The spectrum results are reported upon in detail in [21]. On large length scales, the simulation data is highly-relevant for the plasma around intracluster medium (ICM) shocks ( $\mathcal{M} = u_0/c_s \approx 2$ , where  $c_s$  the sound speed and  $u_0$  is the turbulent velocity dispersion), and the warm and cold phase of the interstellar medium (ISM) of our Galaxy ( $\mathcal{M} \approx 2$ -10) [22, 23], and on small length scales, the plasma becomes weakly-compressible, with  $\mathcal{M} < 1$ , more similar to Earth’s magnetosheath [14, 24] and the solar wind [25]. Hence, these simulations provide orders of magnitudes of scale-dependent statistics, across a broad range of turbulence regimes, with a  $\mathcal{E}_{\text{kin}}(k) \propto k^{-3/2}$  subsonic cascade that is uninfluenced by either the large-scale forcing, or the small-scale dissipation.

## II. NUMERICAL SIMULATION

*MHD model and numerics:* We use a modified version of the magnetohydrodynamical (MHD) code FLASH [26, 27]. Our code uses a highly-optimized, hybrid-precision [28], positivity-preserving, second-order MUSCL-Hancock HLL5R Riemann scheme [29, 30] to solve the isothermal, compressible, ideal, MHD fluid equations in three dimensions. We discretize the equations over a triply periodic domain of  $[-L/2, L/2]$  in each dimension, with  $10,080^3$  grid cells – presently the largest grids in the world for simulations for this turbulence regime. In order to drive turbulence, a turbulent forcing term is applied in the momentum equation (details below). This simulation was run on the supercomputer SuperMUC-NG, utilizing close to 140,000 compute cores and  $8 \times 10^7$ -core hours. We provide more details about the Reynolds number estimates from the numerical diffusion operators in Appendix A, showing that on a  $10,080^3$  grid the simulation has an effective  $\text{Re} \sim \text{Rm} \sim 10^6$ . The turbulence is  $H_m = H_c = 0$ , on  $L$ , but as we find, it is rich in helical fluctuations on smaller scales.

*Turbulent driving:* We drive the turbulence with  $\mathcal{M} = 4.32 \pm 0.18 \approx 4$  to ensure that we resolve a sufficient range of both supersonic  $\mathcal{M} > 1$  and subsonic

$\mathcal{M} < 1$  scales [28]. We apply a non-helical stochastic forcing term isotropically with a parabolic spectrum on  $1 \leq kL/2\pi \leq 3$  wavenumbers, in the momentum equation, following a finite correlation time Ornstein-Uhlenbeck stochastic process [31–33], using the TURB-GEN turbulent forcing module [33, 34]. The correlation time is set to the eddy turnover time on the injection scale. To replenish the large-scale compressible modes, we drive the turbulence with equal amounts of energy in both compressible and incompressible modes [33].

*Magnetization:* In our simulations,  $\langle \mathbf{b} \rangle_{\mathcal{V}} = 0$ , i.e., there is no net magnetic flux through  $\mathcal{V}$  and only a turbulent magnetic field exists. The field is maintained in the saturated state of the turbulent dynamo [18, 19] such that  $\mathcal{E}_{\text{mag}}/\mathcal{E}_{\text{kin}} = 0.242 \pm 0.022 \approx 1/4$ , where  $\mathcal{E}_{\text{mag}}$  and  $\mathcal{E}_{\text{kin}}$  are the volume integral magnetic and kinetic energy. For more information on the initial conditions for  $\mathbf{b}$ , see Appendix B.

## III. THE GLOBAL ALIGNMENT STATISTICS FOR COMPRESSIBLE TURBULENCE

We show a two-dimensional slice of the angle  $\theta_{\mathbf{u},\mathbf{b}}$  between  $\mathbf{u}$  and  $\mathbf{b}$ , for the  $10,080^3$  simulation in Figure 1, showing volume-filling  $\mathbf{u} \propto \pm \mathbf{b}$  states, and volume-poor  $\mathbf{u} \perp \mathbf{b}$  states, suggesting that local regions of the plasma become very strongly (completely) aligned. Alignment could be from the shearing of counter-propagating shear Alfvén wave packets [5], or come from plasma relaxation, if the relaxation timescale is shorter than the eddy turnover time. Solar wind and terrestrial magnetosheath studies suggest that this is indeed possible, and that the relaxation process happens in localized regions rather than globally in the whole plasma [13, 14], similar to what we see in Figure 1.

To quantify the alignment further, we show the global (panels a-c) for  $\mathbf{u}$ ,  $\mathbf{b}$ ,  $\mathbf{j}$  and  $\boldsymbol{\omega}$  alignment in Figure 2. In general, we find that  $\mathbf{u} \propto \pm \mathbf{b} \propto \pm \mathbf{j} \propto \pm \boldsymbol{\omega}$  states are preferred, with all  $\theta$  probability density functions (a) - (c), showing strongly peaked bimodal distributions around parallel  $\theta = 0$  and anti-parallel  $\theta = \pi$  configurations. The question of whether the processes causing the alignment forms perfectly aligned states or whether there is a minimum angle set by an uncertainty principle [36] is not settled by the analysis presented in this study.

## IV. SCALE-DEPENDENT ALIGNMENT

If  $\mathbf{u}$  and  $\mathbf{b}$  follow a process akin to dynamical alignment, which tends to aligns perpendicular scales of eddies keeping the energy flux constant, it is argued that  $\theta_{\mathbf{u},\mathbf{b}}(\lambda) \sim \lambda^{1/4}$  [1, 5]. We provide details about the exact definitions for this statistics in Appendix C. We provide the  $\theta(\lambda)$  structure functions, where  $\lambda$  is the length-scale perpendicular to the local mean magnetic field (definition in Appendix C) for each of the classical

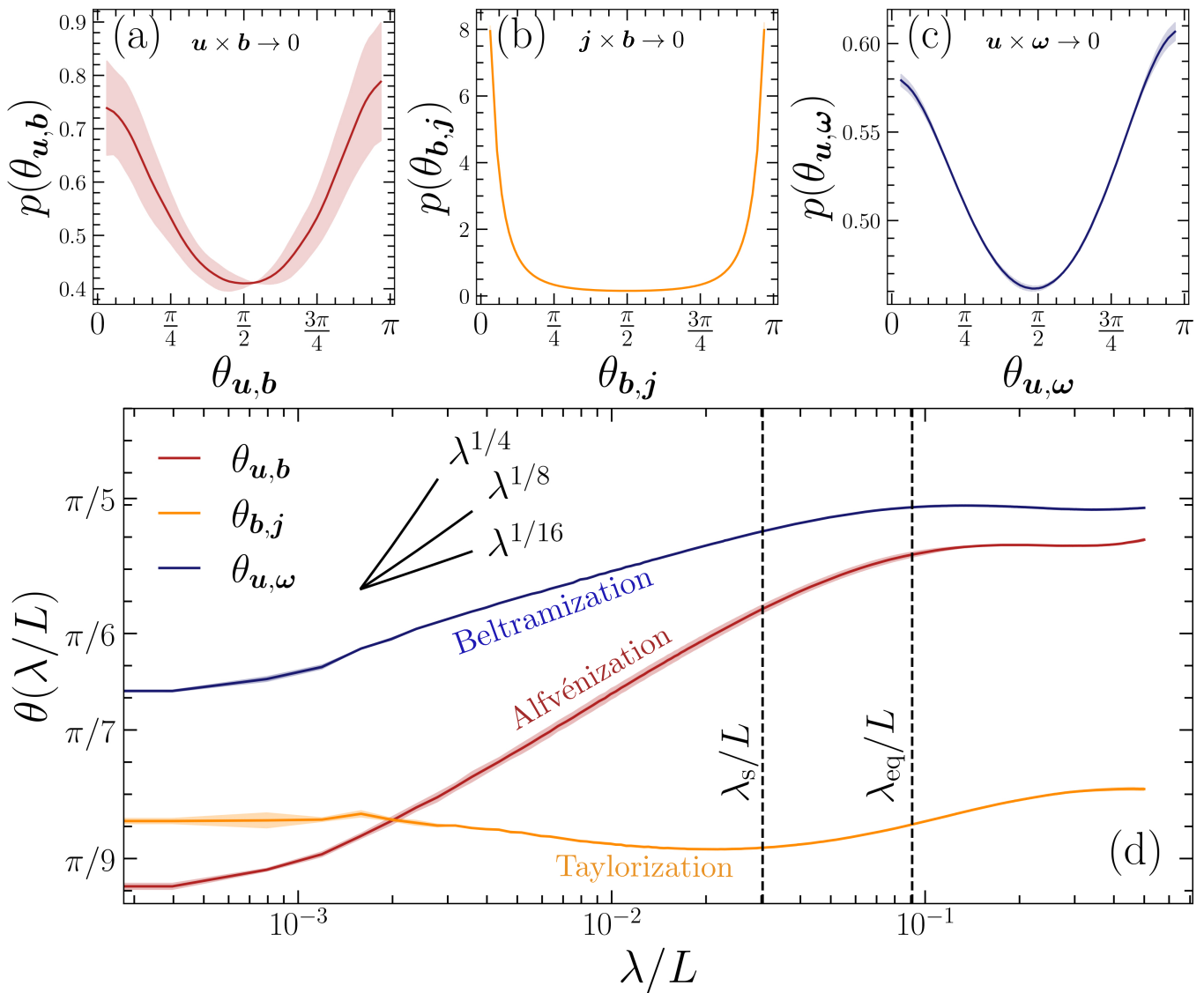


FIG. 2. **The global and scale-dependent alignment statistics of compressible MHD turbulence.** (a)-(c): the one-point distribution functions of  $\theta_{u,b}$ ,  $\theta_{b,j}$  and  $\theta_{u,\omega}$ , all showing bimodal distribution functions peaked at the plasma relaxation states (either parallel or anti-parallel),  $\mathbf{u} \propto \mathbf{b} \propto \mathbf{j} \propto \boldsymbol{\omega}$ , inevitably reducing the strength of the nonlinearities that facilitate the turbulence [14, 15, 35]. (d) the scale-dependent alignment between each of the  $\mathbf{u}$ ,  $\mathbf{b}$ ,  $\mathbf{j}$  and  $\boldsymbol{\omega}$  as a function of local perpendicular length scale  $\lambda$ , with sonic scale  $\lambda_s$  (separating large-scale supersonic velocities from small-scale subsonic velocities; [21, 28]) and energy equipartition scale  $\lambda_{eq}$  (separating large-scale kinetic energy-dominated scales with small-scale magnetically dominated scales; [21]) annotated. Both  $\theta_{u,b} \sim \lambda^{1/8}$  and  $\theta_{u,\omega} \sim \lambda^{1/16}$  show scale dependent alignment at smaller scales than  $\lambda_{eq}$ , indicating that the nonlinearities in both the induction and momentum equation are becoming progressively weaker throughout the highly-magnetized scales of the plasma. The relation,  $\theta_{u,b} \sim \lambda^{1/8}$  is inconsistent with the dynamical alignment prediction  $\theta_{u,b} \sim \lambda^{1/4}$  [1, 2], and is currently unexplained by any turbulence theory. Unlike the other alignments,  $\theta_{b,j}$  exhibits scale-independent alignment, which, coupled with panel (b), means the turbulence is tending toward a globally force-free, Taylor state ( $\mathbf{b} \propto \pm \mathbf{j}$ ), suppressing the Lorentz force on all scales.

relaxation variables, further annotating two important scales. The first is the energy equipartition scale  $\lambda_{eq}$  (the isotropic version of this scale is shown in Figure 1), which is the  $\lambda$  for which  $t_A = t_u$ , where  $t_A = \lambda/v_A(\lambda)$  and  $t_u = \lambda/u(\lambda)$  are the Alfvénic and hydrodynamic timescales. On  $\lambda < \lambda_{eq}$ ,  $t_A < t_u$ , and the magnetic field fluctuations can respond to velocity fluctuations, and vice-versa for  $\lambda > \lambda_{eq}$  [21]. The second is the sonic scale,  $\lambda_s$ , where  $\mathcal{M}(\lambda_s) = u(\lambda_s)/c_s = 1$  [28]. Hence on

scales  $\ell < \ell_s$ ,  $\mathcal{M}(\lambda) < 1$  and vice-versa. This shows that on large scales  $\lambda > \lambda_{eq} > \lambda_s$  plasma is hydrodynamic and supersonic, and on small scales  $\lambda < \lambda_{eq} < \lambda_s$  the plasma is magnetically-dominated and subsonic [21].

We find a significant scale-dependent alignment in  $\theta_{u,b}(\lambda) \sim \lambda^{1/8}$  and  $\theta_{u,\omega}(\lambda) \sim \lambda^{1/16}$  starting directly on scales where  $\lambda < \lambda_{eq}$ ,  $t_A < t_u$ , i.e., the typical size-scale of the aligned regions in Figure 1. On  $\lambda > \lambda_{eq}$ , no scale-dependence is found. Hence the region size  $\sim \lambda_{eq}$  is

setting the outer scale of the self-similar alignment structure. The  $\theta_{\mathbf{b},\mathbf{j}}(\lambda)$  structure function is scale-independent, but shows strong alignment across all of the scales in the turbulence, i.e., the mean alignment is close to parallel, and does not change at any scale. This suggests that the plasma tends towards a global force-free state where  $\mathbf{b} \propto \pm \mathbf{j}$  across all scales, on average (noting that these are first-order structure functions). The  $\theta_{\mathbf{u},\mathbf{b}}(\lambda) \sim \lambda^{1/8}$  scaling is inconsistent with the dynamical alignment prediction of Alfvénic MHD turbulence theory [1, 3], and hence a new theory is required to describe this scaling law. Note that a similar  $\theta_{\mathbf{u},\mathbf{b}}(\lambda) \sim \lambda^{1/8}$  scaling has been found in no net flux simulations at much lower  $\text{Re} \sim 800$  [2], which we show here is potentially the asymptotic state, with no steepening to the  $\theta_{\mathbf{u},\mathbf{b}}(\lambda) \sim \lambda^{1/4}$  relation at  $\text{Re} \sim \text{Rm} \gtrsim 10^6$ . This is the first measurement showing that there is a weak scale-dependent alignment between  $\mathbf{u}$  and  $\boldsymbol{\omega}$ , and that the turbulence develops into, on average, a scale-independent Taylor state.

## V. CONCLUSIONS

Utilizing what is presently the largest turbulence simulation in the world, we have shown that in driven, steady-state compressible MHD turbulence with no net flux there are many aspects of the plasma that admit to a tendency of suppression of the nonlinearities that give rise to the turbulence, and a state of balance, both of which are unusual for a strongly nonlinear, chaotic system like MHD turbulence. Furthermore, most of these tendencies become stronger at scales below the  $t_A < t_u$  scale (the Alfvén or energy equipartition scale). Below these scales the turbulence self-organizes into highly-aligned patches, or cells, as we show in Figure 1. Patches of cross-helical  $\sim 1$  AU regions have been shown in measurements of the solar wind and the terrestrial magnetosheath [13, 14, 37], and on all scales in the solar wind [38]. Averaging over the statistics of these patches in the turbulence gives rise to scale-dependent alignment which we show explicitly in Figure 2. Understanding the size scale (to the first order  $\sim \ell_{\text{eq}}$ ) and stability of these relaxed regions (a generalization of the work [39]) will be important in determining the universal features of turbulence in space and astrophysical systems.

The  $\mathbf{u}$ - $\mathbf{b}$  alignment is of particular interest for Alfvénic turbulence. Our scale-dependent alignment structure function reveals  $\theta_{\mathbf{u},\mathbf{b}}(\lambda) \sim \lambda^{1/8}$ , which is inconsistent with the dynamical alignment prediction  $\theta_{\mathbf{u},\mathbf{b}}(\lambda) \sim \lambda^{1/4}$  – a unique scale-dependent alignment result for constant energy flux [1, 3]. However, the new alignment result obtained in this study would imply naively that for a  $k^{-3/2}$  spectrum, the energy cascade rate is *not* scale-independent but given by  $\epsilon \sim \ell^{1/8}$  in our simulation, which has indeed shown to be true for the kinetic energy [21]. Note that  $\theta_{\mathbf{u},\mathbf{b}}(\lambda) \sim \lambda^{1/4}$  is an Alfvénic turbulence model in the presence of an external guide field, which can be described by the reduced MHD (RMHD)

model. The results we present here go beyond the scope of RMHD. However, even no net magnetic flux turbulence has been hypothesized to become asymptotically RMHD at small enough scales [40], before tearing instabilities may change the cascade [20]. We demonstrate that this does not seem to be the case in our simulation, i.e., no-net flux turbulence does not approach the predictions of the RMHD model asymptotically, at least for  $\text{Re} \sim \text{Rm} \gtrsim 10^6$ . Furthermore, with weaker scale-dependent alignment, this means that the onset of a tearing-mediated cascade,  $\lambda < \lambda_*$ , is at even greater  $\text{Rm}$  than the prediction for the RMHD case,  $k_* \sim \text{Rm}^{4/7}$  [10–12]. Following [11], for  $\lambda/\xi \sim \ell^{1/8}$ , we get  $k_* \sim \text{Rm}^{5/4}$ , or in other words, a factor  $\sim \text{Rm}^{19/28}$  towards higher  $k$ . For  $k_* \sim 10^3$  at  $\text{Rm} \sim 10^5$  in [12], we would have  $k_* \sim 10^6$ , requiring a  $\sim (10^7)^3$  simulation, outside the range of computational tractability on modern supercomputers.

There are immediate difficulties in applying any classical relaxation theory to a stochastic system that has zero  $H_m$  and  $H_c$  on the system scale [41]. Hence, this study leaves an open question as to how to approach the problem of scale-dependent relaxation and the nature of local,  $\langle \dots \rangle_{\ell^3}$ , conservation of rugged invariants such as  $H_{m,\ell}$  and  $H_{c,\ell}$ , or relaxation with more complex and recent invariants, such as the Hosking integral [41]. We, however, stress its importance for making future progress on determining size scales of relaxed regions, which sets the outer-scale for the scale-dependent alignment, as well as scaling relations for the angle structure functions and potentially even spectrum, which are reported in [21].

The question remains: What is the asymptotic state of turbulence if it tends to suppress its nonlinearities as one moves deeper into the cascade? For Kolmogorov turbulence,  $\text{Re}(k) \sim k^{-4/3}$ , and hence  $\text{Re}/\theta_{\mathbf{u},\mathbf{b}} \sim k^{-29/24}$ , which means  $\text{Re}$  shrinks faster than the nonlinearity depletes (the same holds for each of the  $\theta$ , and using a  $k^{-3/2}$  spectrum,  $\text{Re}(k) \sim k^{-5/4}$ ). Hence at asymptotically large  $\text{Re}$ , the cascade is viscously truncated faster than it is nonlinearly depleted, or in other words, the alignment may change the spectral slope of the cascade, but it does not change its fundamental persistence. Regardless, naively based on our results, at some high yet intermediate  $\text{Re}$  and  $\text{Rm}$ , it appears that MHD turbulence tends to become increasingly hydrodynamical in the cascade, with the scale-dependent Taylorization ( $\mathbf{b} \propto \pm \mathbf{j}$ ) and Alfvénization ( $\mathbf{b} \propto \pm \mathbf{u}$ ), hydrodynamizing the MHD equations faster than the Beltramization ( $\mathbf{u} \propto \pm \boldsymbol{\omega}$ ) of the plasma, as we show in Figure 2. Then at even higher  $\text{Re}$  and  $\text{Rm}$ , the plasma tends to become Beltramized too, still with hydrodynamical nonlinearity  $\mathbf{u} \cdot \nabla \otimes \mathbf{u} \approx (1/2)\nabla u^2$ , but potentially with a depleted cascade compared to the Kolmogorov prediction. This is a drastic yet direct outcome of alignment being spread not just across  $\mathbf{u}$  and  $\mathbf{b}$ , but all primitive variables and their curls in the turbulent MHD plasma.

## ACKNOWLEDGMENTS

J. R. B. acknowledges the support from Christoph Federrath, whose help and guidance made it possible to perform the calculations at these scales. Further, we acknowledge the productive discussions with Ralf S. Klessen, Salvatore Cielo, Riddhi Bandyopadhyay, Eliot Quataert, Sasha Philippov, Philipp K. S. Kempster,

Drummond Fielding, Alexander Chernoglazov, Philip Mocz, Bart Ripperda and Chris Thompson. **Funding:** J. R. B. further acknowledges high-performance computing resources provided by the Leibniz Rechenzentrum and the Gauss Centre for Supercomputing grants pr73fi, pn76gi and pn76ga, and GCS large-scale project 10391. J. R. B. and A. B further acknowledge the support from NSF Award 2206756.

- 
- [1] S. Boldyrev, Spectrum of magnetohydrodynamic turbulence, *Physical Review Letters* **96**, 115002 (2006).
- [2] J. Mason, F. Cattaneo, and S. Boldyrev, Dynamic Alignment in Driven Magnetohydrodynamic Turbulence, *Phys. Rev. Lett.* **97**, 255002 (2006), arXiv:astro-ph/0602382 [astro-ph].
- [3] J. C. Perez and S. Boldyrev, Role of Cross-Helicity in Magnetohydrodynamic Turbulence, *Physical Review Letters* **102**, 025003 (2009), arXiv:0807.2635 [astro-ph].
- [4] A. Mallet, A. A. Schekochihin, and B. D. G. Chandran, Refined critical balance in strong Alfvénic turbulence., *The Monthly Notices of The Royal Astronomical Society* **449**, L77 (2015), arXiv:1406.5658 [astro-ph.SR].
- [5] B. D. G. Chandran, A. A. Schekochihin, and A. Mallet, Intermittency and Alignment in Strong RMHD Turbulence, *Astrophys. J.* **807**, 39 (2015), arXiv:1403.6354 [astro-ph.SR].
- [6] A. Chernoglazov, B. Ripperda, and A. Philippov, Dynamic Alignment and Plasmoid Formation in Relativistic Magnetohydrodynamic Turbulence, *The Astrophysical Journal Letters* **923**, L13 (2021), arXiv:2111.08188 [astro-ph.HE].
- [7] N. Sioulas, M. Velli, A. Mallet, T. A. Bowen, B. D. G. Chandran, C. Shi, S. S. Cerri, I. Liodis, T. Ervin, and D. E. Larson, Scale-Dependent Dynamic Alignment in MHD Turbulence: Insights into Intermittency, Compressibility, and Imbalance Effects, arXiv e-prints , arXiv:2407.03649 (2024), arXiv:2407.03649 [physics.space-ph].
- [8] M. Dobrowolny, A. Mangeney, and P. Veltri, Properties of magnetohydrodynamic turbulence in the solar wind, *Astronomy and Astrophysics* **83**, 26 (1980).
- [9] A. Mallet and A. A. Schekochihin, A statistical model of three-dimensional anisotropy and intermittency in strong Alfvénic turbulence, *The Monthly Notices of The Royal Astronomical Society* **466**, 3918 (2017), arXiv:1606.00466 [physics.space-ph].
- [10] N. F. Loureiro and S. Boldyrev, Role of Magnetic Reconnection in Magnetohydrodynamic Turbulence, *Physical Review Letters* **118**, 245101 (2017), arXiv:1612.07266 [physics.plasm-ph].
- [11] L. Comisso, Y. M. Huang, M. Lingam, E. Hirvijoki, and A. Bhattacharjee, Magnetohydrodynamic Turbulence in the Plasmoid-mediated Regime, *The Astrophysical Journal* **854**, 103 (2018), arXiv:1802.02256 [physics.plasm-ph].
- [12] C. Dong, L. Wang, Y.-M. Huang, L. Comisso, T. A. Sandstrom, and A. Bhattacharjee, Reconnection-driven energy cascade in magnetohydrodynamic turbulence, *Science Advances* **8**, eabn7627 (2022), arXiv:2210.10736 [astro-ph.SR].
- [13] W. H. Matthaeus, A. Pouquet, P. D. Mininni, P. Dmitruk, and B. Breech, Rapid Alignment of Velocity and Magnetic Field in Magnetohydrodynamic Turbulence, *Physical Review Letters* **100**, 085003 (2008), arXiv:0708.0801 [astro-ph].
- [14] F. Pecora, Y. Yang, A. Chasapis, S. Servidio, M. E. Cuesta, S. Roy, R. Chhiber, R. Bandyopadhyay, D. J. Gershman, B. L. Giles, J. L. Burch, and W. H. Matthaeus, Relaxation of the turbulent magnetosheath, *The Monthly Notices of The Royal Astronomical Society* **525**, 67 (2023), arXiv:2302.00634 [physics.flu-dyn].
- [15] S. Banerjee, A. Halder, and N. Pan, Universal turbulent relaxation of fluids and plasmas by the principle of vanishing nonlinear transfers, *Physical Review E* **107**, L043201 (2023), arXiv:2209.12735 [physics.plasm-ph].
- [16] J. B. Taylor, Relaxation of toroidal plasma and generation of reverse magnetic fields, *Phys. Rev. Lett.* **33**, 1139 (1974).
- [17] A. N. Kolmogorov, The local structure of turbulence in incompressible viscous fluid for very large Reynolds numbers, *Doklady Akademii Nauk Sssr* **30**, 301 (1941).
- [18] A. A. Schekochihin, S. C. Cowley, G. W. Hammett, J. L. Maron, and J. C. McWilliams, A model of nonlinear evolution and saturation of the turbulent MHD dynamo, *New Journal of Physics* **4**, 84 (2002).
- [19] A. A. Schekochihin, S. C. Cowley, S. F. Taylor, J. L. Maron, and J. C. McWilliams, Simulations of the small-scale turbulent dynamo, *The Astrophysical Journal* **612**, 276 (2004).
- [20] A. K. Galishnikova, M. W. Kunz, and A. A. Schekochihin, Tearing Instability and Current-Sheet Disruption in the Turbulent Dynamo, *Physical Review X* **12**, 041027 (2022), arXiv:2201.07757 [astro-ph.HE].
- [21] J. R. Beattie, C. Federrath, R. S. Klessen, S. Cielo, and A. Bhattacharjee, The spectrum of magnetized turbulence in the interstellar medium, arXiv e-prints , arXiv:2504.07136 (2025), arXiv:2504.07136 [astro-ph.GA].
- [22] B. M. Gaensler, M. Haverkorn, B. Burkhart, K. J. Newton-McGee, R. D. Ekers, A. Lazarian, N. M. McClure-Griffiths, T. Robishaw, J. M. Dickey, and A. J. Green, Low-Mach-number turbulence in interstellar gas revealed by radio polarization gradients, *Nature (London)* **478**, 214 (2011), arXiv:1110.2896 [astro-ph.GA].
- [23] C. Federrath, J. M. Rathborne, S. N. Longmore, J. M. D. Kruijssen, J. Bally, Y. Contreras, R. M. Crocker, G. Garay, J. M. Jackson, L. Testi, and A. J. Walsh, The Link between Turbulence, Magnetic Fields, Filaments, and Star Formation in the Central Molecular Zone

- Cloud G0.253+0.016, *The Astrophysical Journal* **832**, 143 (2016), arXiv:1609.05911 [astro-ph.GA].
- [24] R. Bandyopadhyay, J. R. Beattie, and A. Bhattacharjee, Density fluctuation-Mach number scaling in compressible, high plasma beta turbulence: in-situ space observations and high-Reynolds number simulations, arXiv e-prints , arXiv:2502.08883 (2025), arXiv:2502.08883 [astro-ph.SR].
- [25] A. Bhattacharjee, C. S. Ng, and S. R. Spangler, Weakly Compressible Magnetohydrodynamic Turbulence in the Solar Wind and the Interstellar Medium, *The Astrophysical Journal* **494**, 409 (1998).
- [26] B. Fryxell, K. Olson, P. Ricker, F. X. Timmes, M. Zingales, D. Q. Lamb, P. MacNeice, R. Rosner, J. W. Truran, and H. Tufo, FLASH: An Adaptive Mesh Hydrodynamics Code for Modeling Astrophysical Thermonuclear Flashes, *The Astrophysical Journal Supplement* **131**, 273 (2000).
- [27] A. Dubey, R. Fisher, C. Graziani, G. C. Jordan, IV, D. Q. Lamb, L. B. Reid, P. Rich, D. Sheeler, D. Townsley, and K. Weide, Challenges of Extreme Computing using the FLASH code, in *Numerical Modeling of Space Plasma Flows*, Astronomical Society of the Pacific Conference Series, Vol. 385, edited by N. V. Pogorelov, E. Audit, and G. P. Zank (2008) p. 145.
- [28] C. Federrath, R. S. Klessen, L. Iapichino, and J. R. Beattie, The sonic scale of interstellar turbulence, *Nature Astronomy* 10.1038/s41550-020-01282-z (2021).
- [29] F. Bouchut, C. Klingenberg, and K. Waagan, A multi-wave approximate riemann solver for ideal mhd based on relaxation ii: numerical implementation with 3 and 5 waves, *Numerische Mathematik* **115**, 647 (2010).
- [30] K. Waagan, C. Federrath, and C. Klingenberg, A robust numerical scheme for highly compressible magnetohydrodynamics: Nonlinear stability, implementation and tests, *Journal of Computational Physics* **230**, 3331 (2011), arXiv:1101.3007 [astro-ph.IM].
- [31] V. Eswaran and S. B. Pope, An examination of forcing in direct numerical simulations of turbulence, *Computers and Fluids* **16**, 257 (1988).
- [32] W. Schmidt, C. Federrath, M. Hupp, S. Kern, and J. C. Niemeyer, Numerical simulations of compressively driven interstellar turbulence. I. Isothermal gas, *Astronomy and Astrophysics* **494**, 127 (2009), arXiv:0809.1321 [astro-ph].
- [33] C. Federrath, J. Roman-Duval, R. Klessen, W. Schmidt, and M. M. Mac Low, Comparing the statistics of interstellar turbulence in simulations and observations: Solenoidal versus compressive turbulence forcing, *Astronomy and Astrophysics* **512**, 10.1051/0004-6361/200912437 (2010), arXiv:0905.1060.
- [34] C. Federrath, J. Roman-Duval, R. S. Klessen, W. Schmidt, and M. M. Mac Low, TG: Turbulence Generator, *Astrophysics Source Code Library*, record ascl:2204.001 (2022), ascl:2204.001.
- [35] T. Stribling and W. H. Matthaeus, Relaxation processes in a low-order three-dimensional magnetohydrodynamics model, *Physics of Fluids B: Plasma Physics* **3**, 1848 (1991), [https://pubs.aip.org/aip/pfb/article-pdf/3/8/1848/12367716/1848.1\\_online.pdf](https://pubs.aip.org/aip/pfb/article-pdf/3/8/1848/12367716/1848.1_online.pdf).
- [36] S. Boldyrev, On the Spectrum of Magnetohydrodynamic Turbulence, *The Astrophysical Journal Letters* **626**, L37 (2005), arXiv:astro-ph/0503053 [astro-ph].
- [37] K. T. Osman, M. Wan, W. H. Matthaeus, B. Breech, and S. Oughton, Directional Alignment and Non-Gaussian Statistics in Solar Wind Turbulence, *The Astrophysical Journal* **741**, 75 (2011).
- [38] C. H. K. Chen, S. D. Bale, C. S. Salem, and B. A. Maruca, Residual Energy Spectrum of Solar Wind Turbulence, *Astrophys. J.* **770**, 125 (2013), arXiv:1304.7818 [physics.space-ph].
- [39] D. N. Hosking, A. A. Schekochihin, and S. A. Balbus, Elasticity of tangled magnetic fields, *Journal of Plasma Physics* **86**, 905860511 (2020), arXiv:2006.15141 [astro-ph.HE].
- [40] A. A. Schekochihin, MHD turbulence: a biased review, *Journal of Plasma Physics* **88**, 155880501 (2022), arXiv:2010.00699 [physics.plasm-ph].
- [41] D. N. Hosking and A. A. Schekochihin, Reconnection-controlled decay of magnetohydrodynamic turbulence and the role of invariants, *Phys. Rev. X* **11**, 041005 (2021).
- [42] N. Kriel, J. R. Beattie, A. Seta, and C. Federrath, Fundamental scales in the kinematic phase of the turbulent dynamo, *The Monthly Notices of The Royal Astronomical Society* **513**, 2457 (2022), arXiv:2204.00828 [astro-ph.SR].
- [43] P. Grete, B. W. O'Shea, and K. Beckwith, As a Matter of Dynamical Range - Scale Dependent Energy Dynamics in MHD Turbulence, *The Astrophysical Journal Letters* **942**, L34 (2023), arXiv:2211.09750 [astro-ph.GA].
- [44] L. Malvadi Shivakumar and C. Federrath, Numerical viscosity and resistivity in MHD turbulence simulations, arXiv e-prints , arXiv:2311.10350 (2023), arXiv:2311.10350 [astro-ph.SR].
- [45] J. R. Beattie, C. Federrath, N. Kriel, P. Mocz, and A. Seta, Growth or Decay - I: universality of the turbulent dynamo saturation, *The Monthly Notices of The Royal Astronomical Society* **524**, 3201 (2023), arXiv:2209.10749 [astro-ph.GA].
- [46] A. Seta and C. Federrath, Seed magnetic fields in turbulent small-scale dynamos, *The Monthly Notices of The Royal Astronomical Society* **499**, 2076 (2020), arXiv:2009.12024 [astro-ph.GA].
- [47] F. Rincon, Dynamo theories, *Journal of Plasma Physics* **85**, 205850401 (2019), arXiv:1903.07829 [physics.plasm-ph].
- [48] D. J. Price and C. Federrath, A comparison between grid and particle methods on the statistics of driven, supersonic, isothermal turbulence, *The Monthly Notices of The Royal Astronomical Society* **406**, 1659 (2010), arXiv:1004.1446 [astro-ph.GA].
- [49] J. R. Beattie, P. Mocz, C. Federrath, and R. S. Klessen, The density distribution and physical origins of intermittency in supersonic, highly magnetized turbulence with diverse modes of driving, *The Monthly Notices of The Royal Astronomical Society* **517**, 5003 (2022), arXiv:2109.10470 [astro-ph.GA].

## Appendix A: Estimating the Reynolds numbers

Our numerical model is an implicit large eddy simulation (ILES), which relies upon the spatial discretisation to supply the numerical viscosity and resistivity as a fluid closure model. Recently, a detailed characterization of the numerical viscous and resistive properties, specifically for turbulent boxes, has been performed on this code by comparing the ILES model with direct numerical simulations (DNS), which have explicit viscous and resistive operators [42–44]. [43] showed that a ILES turbulence is exactly equivalent to a DNS at a specific set of viscous and resistive coefficients. Furthermore, Malvadi Shivakumar and Federrath [44] derived empirical models for transforming grid resolution  $N_{\text{grid}}$  into Re and Rm. For supersonic MHD turbulence, they find,  $\text{Re} = (N_{\text{grid}}/N_{\text{Re}})^{p_{\text{Re}}}$ , where  $p_{\text{Re}} \in [1.5, 2.0]$  and  $N_{\text{Re}} \in [0.8, 4.4]$  and  $\text{Rm} = (N_{\text{grid}}/N_{\text{Rm}})^{p_{\text{Rm}}}$ , where  $p_{\text{Rm}} \in [1.2, 1.6]$  and  $N_{\text{Rm}} \in [0.1, 0.7]$ . For our  $N_{\text{grid}} = 10,080$  simulation, this gives  $\text{Re} \in [1.4 \times 10^6, 5.3 \times 10^6]$  and  $\text{Rm} \in [1 \times 10^6, 4.5 \times 10^6]$ . This is the Re and Rm we report in the main text.

## Appendix B: Initial conditions and hierarchical interpolation

Regardless of the initial field amplitude or structure, the same small-scale dynamo saturation is reached [45, 46]. Hence, given enough integration time, we can initialize a  $\mathbf{b}$  with any initial structure and amplitude and be confident that it will result in the same saturation. However, to minimize the computational resources on the fast or nonlinear dynamo stages [42, 47], we initialize the  $\mathbf{b}$  amplitude and structure close to the saturated state. From our previous experiments at lower resolutions, this is  $\mathcal{E}_{\text{mag}}/\mathcal{E}_{\text{kin}} \approx 1/4$  (or Alfvén Mach number  $\mathcal{M}_A \approx 2$ ), and with a significant amount of power at all  $k$ . We find that a uniform initial  $\mathcal{E}_{\text{mag}}(k)$ , with sufficiently high  $k$  modes included, relaxes very quickly to the saturated dynamo state. Hence we use a simple, isotropic uniform top-hat spectrum within  $1 \leq kL/2\pi \leq 50$ , which is generated as a divergence-free, static, random field using TURBGEN [33, 34].

Driven MHD turbulence in this regime requires  $\approx (1-2)t_0$ , where  $t_0 = \ell_0/u_0$  is the turbulent turnover time on the outer scale, to remove the influence of its initial conditions and establish a stationary state [33, 48, 49]. To avoid expending compute resources on simulating this transient state, we only apply the previously discussed initial conditions to a  $2,520^3$  simulation and drive it into a steady state. We use the steady state as an initial condition for a  $5,040^3$  simulation, drive it to a steady state, and then finally we interpolate it to the  $10,080^3$  simulation. We drive continuously for  $2t_0$  in the steady state and compute all of the statistics we use in the main text averaged over 10 realizations. We use linear interpolation to preserve  $\nabla \cdot \mathbf{b} = 0$  between grid interpolations. It takes

a tiny fraction of  $t_0$ ,  $t \sim \text{Re}^{-1/2}t_0$ , to populate the new modes after the interpolation onto the higher-resolution grid.

## Appendix C: Definitions of scale-dependent alignment structure functions

To compute the scale-dependent alignment structure function shown in Figure 2 (d), we first define our increments,

$$\delta \mathbf{u} = \mathbf{u}(\mathbf{r}) - \mathbf{u}(\mathbf{r} + \boldsymbol{\ell}), \quad (\text{C1})$$

$$\delta \mathbf{b} = \mathbf{b}(\mathbf{r}) - \mathbf{b}(\mathbf{r} + \boldsymbol{\ell}), \quad (\text{C2})$$

for separation vector  $\boldsymbol{\ell}$ . Next, we define a local mean magnetic field direction,

$$\widehat{\mathbf{b}}_{\boldsymbol{\ell}} = \frac{\mathbf{b}(\mathbf{r}) + \mathbf{b}(\mathbf{r} + \boldsymbol{\ell})}{\|\mathbf{b}(\mathbf{r}) + \mathbf{b}(\mathbf{r} + \boldsymbol{\ell})\|}, \quad (\text{C3})$$

and then find the perpendicular component to the local field for each of the fluid variables, e.g. for  $\mathbf{u}$  and  $\mathbf{b}$ ,

$$\delta \mathbf{u}_{\lambda} = \delta \mathbf{u} - (\delta \mathbf{u} \cdot \widehat{\mathbf{b}}_{\boldsymbol{\ell}}) \widehat{\mathbf{b}}_{\boldsymbol{\ell}}, \quad (\text{C4})$$

$$\delta \mathbf{b}_{\lambda} = \delta \mathbf{b} - (\delta \mathbf{b} \cdot \widehat{\mathbf{b}}_{\boldsymbol{\ell}}) \widehat{\mathbf{b}}_{\boldsymbol{\ell}}, \quad (\text{C5})$$

which is the standard definition for these quantities [6, 12]. Next, we construct the ratio between first-order structure functions,

$$\theta_{\mathbf{u},\mathbf{b}}(\lambda) \sim |\sin \theta_{\mathbf{u},\mathbf{b}}(\lambda)| = \frac{\langle |\delta \mathbf{u}_{\lambda} \times \delta \mathbf{b}_{\lambda}| \rangle_{\boldsymbol{\ell}}}{\langle |\delta \mathbf{u}_{\lambda}| |\delta \mathbf{b}_{\lambda}| \rangle_{\boldsymbol{\ell}}}. \quad (\text{C6})$$

We do this for each pair of relaxation variables  $\mathbf{u}$  and  $\mathbf{b}$ ,  $\mathbf{j}$  and  $\mathbf{b}$ , and lastly  $\boldsymbol{\omega}$  and  $\mathbf{u}$ . We use  $2 \times 10^{12}$  sampling pairs to ensure that the structure functions converge on all scales [28]. Furthermore, we construct the structure functions across a number of realizations in the stationary state and then time-average the structure function to produce Figure 2.

## Appendix D: Critical length scale for tearing-mediated cascade

Starting at Equation (8) in [11], we define the critical perpendicular length scale ratio,

$$\frac{\lambda_*}{\xi_*} = \left[ \frac{\bar{\alpha}}{S_{\xi}^{1/2} W(\zeta)} \right]^{2/3}, \quad (\text{D1})$$

where  $S_{\xi} = \xi v_{A,\lambda}/\eta$  is the Lundquist number defined on  $\xi$  with  $v_{A,\lambda}$ ,  $W(\zeta)$  is a Lambert W function, and  $\bar{\alpha}$  is linear function of the spectral exponent for the perturbative noise spectrum. The argument for the  $W$  is a function of the noise spectrum and  $S_{\xi}$ . We can write,

$$\lambda_* = \left[ \frac{\bar{\alpha}}{S_{\xi}^{1/2} W(\zeta)} \right]^{16/3}, \quad (\text{D2})$$

utilizing  $\sin \theta_{\mathbf{u}, \mathbf{b}} \sim \lambda_*/\xi_* \sim \lambda_*^{1/8}$ , the scale-dependent relation we find in this study. Likewise, using this relation

to modify  $S_\xi$ , we get

$$S_\xi^{1/2} = \left( \frac{\lambda_*^{7/8}}{L} \text{Rm} \right)^{1/2} = \frac{\lambda_*^{7/16}}{L^{1/2}} \text{Rm}^{1/2}. \quad (\text{D3})$$

and substituting back in Equation (D2),

$$\frac{\lambda_*}{L} \sim \text{Rm}^{-5/4}, \quad (\text{D4})$$

which we discuss in the main text.